13th World Conference on Earthquake Engineering
Vancouver, B.C., Canada
August 1-6, 2004
Paper No. 1617

HYSTERETIC MODELS FOR ELASTOMER STRUCTURAL DAMPERS AND APPLICATION TO NON-DUCTILE RC FRAME BUILDING

Kyung-Sik LEE[1], Richard SAUSE[2], James RICLES[3], Kamarudin AB-MALEK[4], and Le-Wu LU[5]

SUMMARY

A new elastomer (rubber-like) damping material, ultra high damping natural rubber (UHDNR), has been developed for structural dampers to overcome the limitations of typical viscoelastic (VE) materials. To simulate the hysteretic stress-strain behavior of the elastomer, a loading rate-independent and a loading rate-dependent hysteretic models were developed. The loading rate-dependent model was found to predict well the cyclic behavior of UHDNR dampers subject to a harmonic loading history. To illustrate the application of UHDNR dampers to improve the seismic performance of non-ductile RC frame buildings, a retrofit study of a prototype non-ductile RC frame building was conducted. A simplified design procedure (SDP) for multi-degree-of-freedom (MDOF) frame buildings with dampers is presented. Accurate nonlinear dynamic time history analysis (NDTHA) results are given. Compared to VE dampers, which can be quite sensitive to loading frequency and ambient temperature, the UHDNR dampers reduce the seismic response more effectively when a range of design temperature is considered.

INTRODUCTION

Viscoelastic (VE) dampers have been shown to significantly decrease lateral drift, base shear, and overturning moment during earthquakes (Chang [1], Kasai [2], Fan [3]). However, the mechanical properties (stiffness and damping) of VE materials are usually dependent on ambient temperature, loading frequency, and strain amplitude. Research has shown that the design of structural systems with VE dampers may be not effective or satisfactory if the mechanical properties of the viscoelastic material are highly dependent on these factors (Fan [3], Lee [4]). To overcome this drawback of many VE materials, a new elastomer (rubber-like) damping material, ultra high damping natural rubber (UHDNR), was developed for structural dampers.

The behavior of elastomer damping materials under cyclic loading shows highly nonlinear hysteresis,

[1] Postdoctoral Research Scientist, ATLSS Center, Lehigh Univ., Bethlehem, PA, USA. Email: ksl2@lehigh.edu
[2] Professor of Struct. Eng., ATLSS Center, Lehigh Univ., Bethlehem, PA, USA. Email: rs0c@lehigh.edu
[3] Professor of Struct. Eng., ATLSS Center, Lehigh Univ., Bethlehem, PA, USA. Email: jmr5@lehigh.edu
[4] Research Scientist, Malaysian Rubber Board, Kuala Lumpur, Malaysia. Email: kamarudin@lgm.gov.my
[5] Professor of Civil Eng., ATLSS Center, Lehigh Univ., Bethlehem, PA, USA. Email: lwl0@lehigh.edu

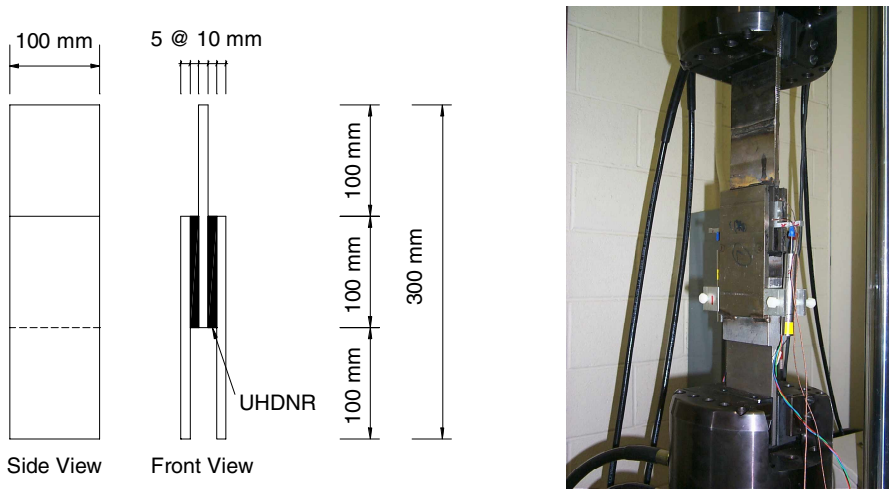

(a) Configuration of structural damper (b) Experimental setup

Fig. 1 UHDNR damper and test setup

mainly dependent on strain amplitude, rather than loading frequency. Therefore, a good representation of the hysteretic behavior of elastomer dampers is essential to accurately estimate the overall response of structures with elastomer dampers. This paper presents hysteretic models developed for elastomer dampers and an application of elastomer dampers to the seismic retrofit of a non-ductile reinforced concrete frame building.

HYSTERETIC BEHAVIOR OF ELASTOMER DAMPER AND ANALYTICAL MODELS

The UHDNR material is an advanced version of the high damping natural rubber (HDNR) that has been used in the base isolation of structures. Compared to HDNR, the UHDNR has greater energy dissipation capacity with a typical loss factor of 0.35. Fig. 1(a) shows a small-scale structural damper that consists of two layers of UHDNR bonded between three steel plates. These small-scale dampers were fabricated at the Malaysian Rubber Board and tested at the ATLSS Center (Fig. 1(b)) at Lehigh University.

Numerous experiments were performed to investigate the hysteretic shear stress-strain behavior dependent on strain amplitude, ambient temperature, and loading frequency. Fig. 2 shows the shear stress-strain response of UHDNR at different strain amplitudes, ambient temperatures, and loading frequencies. The hysteresis loops show significant dependence on the strain amplitude. At small strain amplitudes, the hysteresis loops are stiffer. As shown in Figs. 2(a) and (b), the ambient temperature also affects the hysteretic behavior. The loading frequency is a less important factor than the strain amplitude and ambient temperature, as shown in Figs. 2(c) and (d).

Rate-independent hysteretic model: polynomial asymptote and power function model (PAPFM)

To simulate the hysteretic behavior of elastomers dependent on the strain amplitude, a loading rate-independent hysteretic model was proposed by Sause *et al.* [5]. The rate-independent hysteretic model, the polynomial asymptote and power function model (PAPFM), is depicted in Fig. 3 and expressed as:

$$\frac{d\tau_{hys}(\gamma)}{d\gamma} = \frac{d\overline{\tau}(\gamma)}{d\gamma}\left[1 + k\left(\frac{e}{e_0}\right)^n\right] \tag{1}$$

where, γ indicates the applied shear strain, $\tau_{hys}(\gamma)$ indicates the hysteretic shear stress, $\overline{\tau}(\gamma)$ is the target asymptote for the loading and unloading directions, $e\,(=\overline{\tau}(\gamma)-\tau_{hys}(\gamma))$ is the stress deviation between $\overline{\tau}(\gamma)$ and the current stress $\tau_{hys}(\gamma)$, $e_0\,(=\overline{\tau}(\gamma_0)-\tau_0)$ is the stress deviation between $\overline{\tau}(\gamma)$ and the stress at

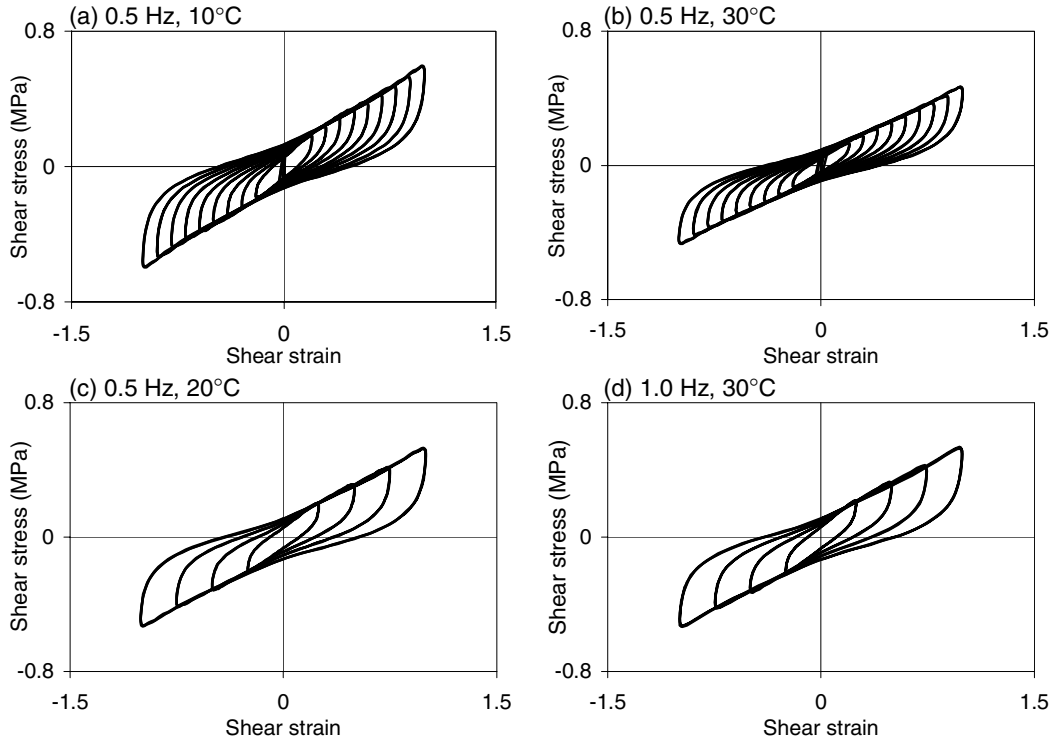

Fig. 2 Hysteretic stress-strain loops

the most recent strain reversal (γ_0, τ_0), and k and n are parameters controlling the sharpness of the hysteresis loop. Eq. (1) implies that the slope of the current stress-strain path asymptotically approaches the slope of the target asymptote $\overline{\tau}(\gamma)$. At any loading reversal points, the slope of the current stress-strain path is the same as the slope of $\overline{\tau}(\gamma)$ multiplied by [1+ k] because (e/e_0) is equal to 1. As $\tau_{hys}(\gamma)$ is close to $\overline{\tau}(\gamma)$, (e/e_0) decreases. Finally (e/e_0) approaches to zero, and $\tau_{hys}(\gamma)$ is very close to $\overline{\tau}(\gamma)$.

Various hysteresis loops can be simulated using Eq. (1) depending on the selection of $\overline{\tau}(\gamma)$. Softening hysteresis can be simulated with a second or fourth order polynomial for $\overline{\tau}(\gamma)$, and hardening hysteresis can be simulated with a third or fifth order polynomial. Nonsymmetrical hysteresis also can be simulated using Eq. (1). $\overline{\tau}(\gamma)$ in Eq. (1) consists of two target asymptotes for the loading direction $\tau_1(\gamma)$ and the target asymptote for the loading direction $\tau_2(\gamma)$. If the hysteresis loops are not symmetric, different

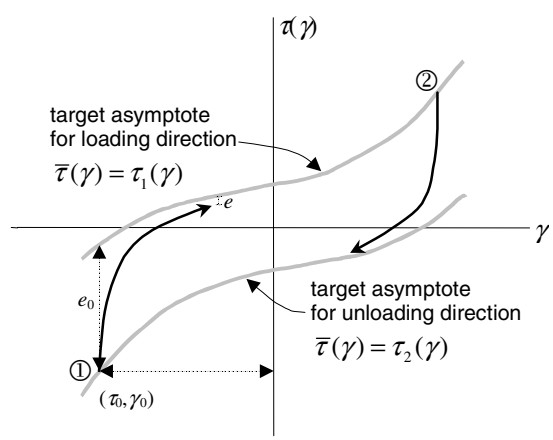

Fig. 3 Schematic of PAPFM

polynomials can be selected for $\tau_1(\gamma)$ and $\tau_2(\gamma)$. In this paper, symmetry of the two target asymptotes about the origin is assumed, since the hysteresis loops of elastomers satisfy this assumption. Then, $\tau_1(\gamma)$ and $\tau_2(\gamma)$ are expressed using a same polynomial with different signs on the coefficients.

For example, when a third order polynomial is considered for $\bar{\tau}(\gamma)$, Eq. (1) for each loading direction can be rewritten as follows:

$$\frac{d\tau_{hys}(\gamma)}{d\gamma}=\frac{d\tau_1(\gamma)}{d\gamma}\left[1+k\left(\frac{e}{e_0}\right)^n\right]=\left(3C_3\gamma^2+2C_2\gamma+C_1\right)\left[1+k\left(\frac{e}{e_0}\right)^n\right] \text{ for the loading direction} \tag{2}$$

$$\frac{d\tau_{hys}(\gamma)}{d\gamma}=\frac{d\tau_2(\gamma)}{d\gamma}\left[1+k\left(\frac{e}{e_0}\right)^n\right]=\left(3C_3\gamma^2-2C_2\gamma+C_1\right)\left[1+k\left(\frac{e}{e_0}\right)^n\right] \text{ for the unloading direction} \tag{3}$$

where, $\tau_1(\gamma)=C_3\gamma^3+C_2\gamma^2+C_1\gamma+C_0$ for the loading direction and $\tau_2(\gamma)=C_3\gamma^3-C_2\gamma^2+C_1\gamma-C_0$ for the unloading direction. Solving Eq. (2) and Eq. (3) for $\tau_{hys}(\gamma)$ yields:

$$\tau_{hys}(\gamma)=\bar{\tau}(\gamma)-e_0\left[1-\frac{\bar{W}(\gamma)k[\gamma_0-\gamma][n-1]}{e_0}\right]^{\frac{1}{1-n}} \tag{4}$$

where, $\bar{W}(\gamma)$ is $W_1(\gamma)=C_3[\gamma^2+\gamma\gamma_0+\gamma_0^2]+C_2[\gamma+\gamma_0]+C_1$ for the loading direction and $W_2(\gamma)=C_3[\gamma^2+\gamma\gamma_0+\gamma_0^2]-C_2[\gamma+\gamma_0]+C_1$ for the unloading direction.

Using Eq. (4), the hysteretic stress $\tau_{hys}(\gamma)$ can be uniquely determined from one strain reversal to the next strain reversal. Eq. (4) is also applicable to other polynomial target asymptotes such as linear, second order, fourth order, and fifth order polynomials. When these polynomials are used as $\bar{\tau}(\gamma)$, the closed-form expression in Eq. (4) remains the same, but $\bar{\tau}(\gamma)$ and $\bar{W}(\gamma)$, which depends on $\bar{\tau}(\gamma)$, differ. The generalized expressions for $\bar{\tau}(\gamma)$ and $\bar{W}(\gamma)$ are, for the loading direction:

$$\bar{\tau}(\gamma)=\tau_1(\gamma)=\sum_{i=0}^{h}\left[C_i\gamma^i\right] \text{ and } \bar{W}(\gamma)=W_1(\gamma)=\sum_{i=1}^{h}\left(C_i\sum_{j=1}^{i}\left[\gamma^{i-j}\gamma_0^{j-1}\right]\right) \tag{5}$$

and for the unloading direction:

$$\bar{\tau}(\gamma)=\tau_2(\gamma)=\sum_{i=0}^{h}\left[(-1)^{i+1}C_i\gamma^i\right] \text{ and } \bar{W}(\gamma)=W_2(\gamma)=\sum_{i=1}^{h}\left((-1)^{i+1}C_i\sum_{j=1}^{i}\left[\gamma^{i-j}\gamma_0^{j-1}\right]\right) \tag{6}$$

where, h is the value of the largest exponent of $\bar{\tau}(\gamma)$.

Rate-dependent hysteretic model

PAPFM was developed for the strain amplitude dependence of elastomers without the consideration of loading frequency. While not distinct in Figs. 2(c) and (d), the hysteretic stress-strain behavior is slightly dependent on the applied loading frequency. A rate-dependent model, a parallel combination of PAPFM and a dashpot, was proposed to capture the loading frequency dependence (Lee [4]) and is expressed as:

$$\tau(\gamma,t)=\tau_{hys}(\gamma)+\tau_{DP}(t) \tag{7}$$

where, $\tau_{hys}(\gamma)$ is PAPFM given by Eq. (4), $\tau_{DP}(t)$ is equal to $c\dot{\gamma}(t)$, and c is the dashpot coefficient. The rate-dependent model in Eq. (7) has several parameters, including the coefficients of the polynomial used for the target asymptote, and k, n, and c.

Parameter estimation

The parameters for the rate-dependent model in Eq. (7) were determined in the shear stress-strain plane satisfying the following least-square condition:

$$\text{Minimize} \left\{ \sum_l \sum_i \sum_j \left[\tau_{\exp}(\gamma_{l,i,j}) - \tau_{\text{mod}}(\gamma_{l,i,j}) \right]^2 \right\} \tag{8}$$

where, l is the index for the experimental data set at a specific frequency (e.g., l = 1, frequency = 0.5 Hz), i is the index for the experimental data set at a specific strain amplitude, j is the index for a stress-strain point within the data set at a specific frequency and strain amplitude, $\tau_{\exp}(\gamma_{l,i,j})$ is the stress data point from the experiments, $\tau_{\text{mod}}(\gamma_{l,i,j})$ is the stress calculated from Eq. (7) using $\gamma_{l,i,j}$, and $\gamma_{l,i,j}$ is the stain data point from the experiments corresponding to $\tau_{\exp}(\gamma_{l,i,j})$. The experimental data was divided into the loading and unloading segments. The Marquardt algorithm (Marquardt [6]) was used to determine the parameters. Details of the parameter estimation can be found in Lee [4].

To consider the ambient temperature effect, nonlinear regressions were performed at different temperatures. Using a fourth order polynomial and n equal to 2, the nonlinear regression was performed at 20°C first, because experiments to investigate the frequency dependence were performed only at 20°C. From this reason, c is assumed to be temperature independent. This assumption is likely to be acceptable because the frequency dependence of UHDNR is not significant. With a constant value of $c=c_{T=20°C}$ in Eq.(7), nonlinear regressions were performed at 0°C, 10°C, 30°C, and 40°C. The parameter values are shown in Table 1.

Using the rate-dependent hysteresis model in Eq. (7), very accurate correlation, as shown in Fig. 4, is obtained between experimental and analytical hysteresis loops at various strain amplitudes, ambient temperatures, and loading frequencies.

Table 1. Parameters determined from nonlinear regression

Ambient Temperature	C_4 (*MPa*)	C_3 (*MPa*)	C_2 (*MPa*)	C_1 (*MPa*)	C_0 (*MPa*)	k	c (*kN -sec/in*)
0°C	-0.274	0.0688	0.304	0.437	0.171	26.599	$c_{T=20°C}$ = 0.0627
10°C	-0.212	0.0990	0.232	0.335	0.127	21.348	
20°C	-0.177	0.0651	0.208	0.316	0.112	21.804	
30°C	-0.163	0.0816	0.178	0.272	0.0873	17.989	
40°C	-0.155	0.0620	0.170	0.272	0.0804	17.083	

RETROFIT OF NON-DUCTILE REINFORCED CONCRETE FRAME BUILDING

To investigate effect of elastomer dampers on the seismic performance of frame buildings, a retrofit study of a prototype non-ductile reinforced concrete (RC) frame building was conducted. The three-story, five-bay by five-bay non-ductile RC frame building (Figs. 5(a) and (b)) is assumed to built in the United States in the 1960's. The prototype building is expected to exhibit poor performance under earthquake loading, because seismic loads were not adequately considered in design (Wu [7]).

Desired seismic performance

The desired seismic performance of the prototype RC frame building with dampers is *operational level* under the design basis earthquake (DBE). Possible brittle failure of the RC frames is to be avoided. To ensure the desired seismic performance, the following design limits for retrofit are imposed; (1) all columns in the original structure should remain elastic when the building is subjected to the DBE along with gravity loads, and (2) the story drifts under the design basis earthquake are limited to 0.4% which is quite small. More attention is focused on the behavior of the columns rather than beams to prevent a story failure mechanism from forming. The drift limit of 0.4% is determined from an inelastic analysis by Wu [7], where extensive inelastic behavior in the first story columns occurs after 0.4% drift.

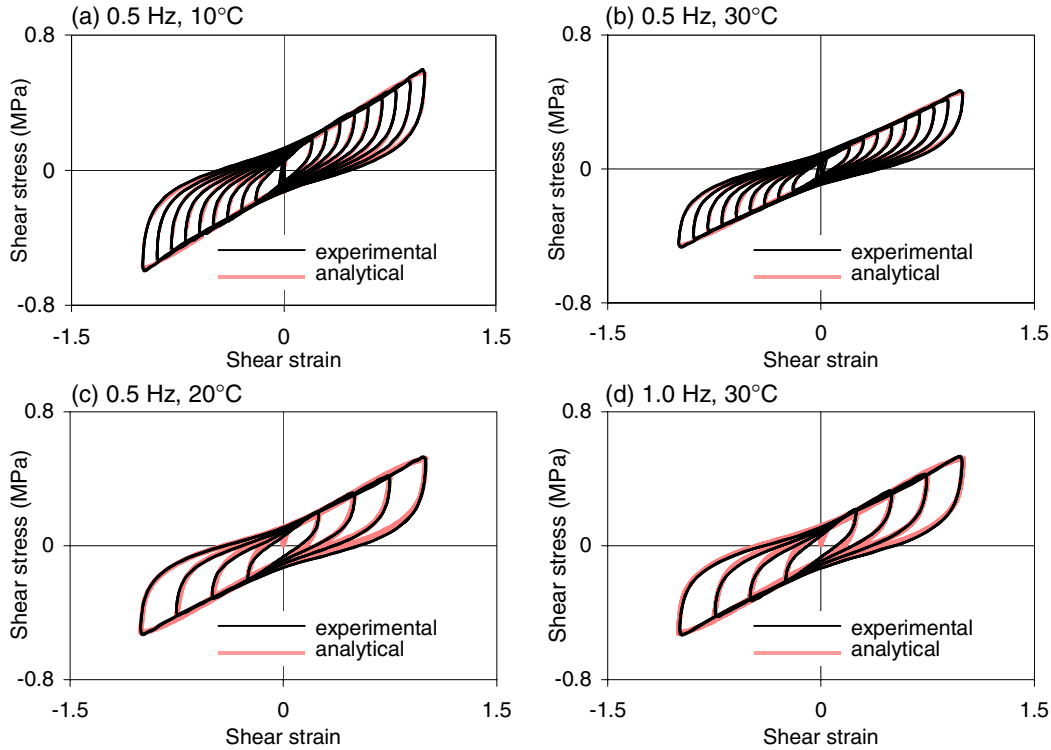

Fig. 4 Comparison of hysteretic stress-strain loops

Analytical models for RC frame with dampers

Fig. 5(c) shows the configuration of dampers and braces for the retrofit of the prototype RC frame building. From symmetry of the building, only three frames are included in the analytical model. Among the three frames, three dampers are located in each story of one of the interior frames, referred to as the interior damped frame. The flexural properties of the beams and columns were evaluated from the moment-curvature analysis results. The bilinear moment-curvature relationships were generated using the RCCOLA program (Farahany [8]). A typical stress-strain relationship for reinforcing steel proposed from

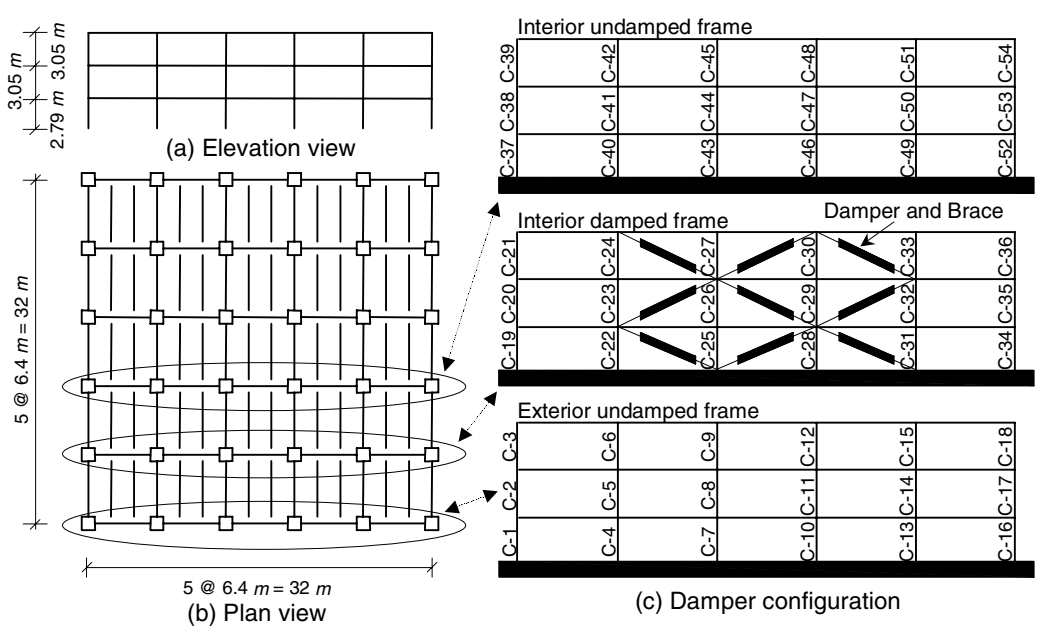

Fig. 5 Prototype non-ductile RC frame building and analytical model

Blume *et al.* [9] was used with an assumed yield stress and ultimate stress for the steel reinforcing bars of 275.8 *MPa* and 482.7 *MPa*. The Kent and Park model [10] was used for the stress-strain relationship of the concrete in compression. Concrete compressive strengths of 25.9 *MPa* for columns and 20.7 *MPa* for beams were used.

Similar to other structural designs, structures with dampers can be designed effectively using a simplified design procedure (SDP) and followed by a more accurate analysis after the simplified design is completed. Damper and brace stiffnesses, which should provide the desired seismic performance, are determined from SDP, which is based on elastic-static analysis. After the simplified design is complete, the seismic performance is verified by a more accurate nonlinear dynamic time history analysis (NDTHA). The SAP-2000 computer program [Habibullah and Wilson [11] was used for SDP. In the SAP-2000 model, elastic beam-column elements were used for the RC columns and beams and elastic truss elements were used for the dampers and braces. The PC-ANSR computer program (Maison [12]) was used for NDTHA. In the PC-ANSR model, nonlinear beam-column elements with bilinear moment-curvature relationship were used for the beams and columns. A 2-node elastomer damper element, with a hysteretic behavior given by Eq. (7) and implemented into PC-ANSR by Lee [4], was used for the elastomer dampers in the PC-ANSR model. A generalized Maxwell element, developed to simulate the stress-strain behavior of viscoelastic (VE) materials and implemented into PC-ANSR by Fan [3], was used for the VE dampers, as discussed later.

Damping materials

In addition to the UHDNR elastomer material, two VE materials were used for the retrofit to compare the performance of the damping materials. ISD-110 is a typical VE material that has been used in experimental and analytical studies of VE dampers in the past (e.g., Chang [1], Kasai [2]). The energy dissipation capacity of ISD-110 material is quite high, however, its mechanical properties highly depend on ambient temperature and loading frequency. KRATON-107 is a VE material with less damping. Its mechanical properties are nearly insensitive to the temperature and frequency (Fan [3]). Typical loss factors are 0.38, 1.30, and 0.29 for the UHDNR, ISD-110, and KRATON-107 materials, respectively.

Simplified design of damped MDOF system

Simplified design procedure (SDP)

A retrofit design for the non-ductile prototype RC frame buildings was performed using the following simplified design procedure (SDP): (1) idealize the nonlinear damping material to a linear VE material, (2) establish desired structural performance and design limits to ensure the desired performance, (3) select a design temperature range, (4) select an appropriate α (stiffness ratio of the brace-to-undamped frame) value, one or more β (stiffness ratio of the damper-to-undamped frame) values, and damper locations, (5) perform elastic-static analysis, (6) compare structural response obtained in Step (5) to the design limits established in Step (2), (7) select a minimum β, (8) determine the structural response at the low-end temperature of the design temperature range and compare to design limits, and (9) calculate the damper area and thickness.

In Step (1), the nonlinear hysteresis loops of elastomer materials such as UHDNR are idealized as a linear viscoelastic ellipse to approximate the equivalent stiffness and damping. The equivalence is obtained using two criteria: (1) the maximum stress and strain are similar and (2) the hysteresis loop area is similar. Step (1) is not necessary for VE materials, such as ISD-110 and KRATON-107.

As discussed earlier, the design limits to ensure the desired seismic performance (*operational*) of the prototype building are elastic behavior of all columns and 0.4% story drift under the DBE. To satisfy the first design limit, the column axial force-moment responses are compared to the factored column axial-

flexural capacity (ϕP_n-ϕM_n). Also the column axial force-shear responses are compared to the factored column axial-shear capacity (ϕP_n-ϕV_n).

An ambient temperature range of 10°C to 30°C was considered in Step (3) as the possible temperature variation in an office building at the time of earthquake. In Step (4), α was assumed equal to 30 because a stiff brace enables the damper to deform more. Values of β equal to 0, 0.1, 0.5, 1, 2, 3, 4, 8, 12, 16, 20, 25, and 30 were considered. Then, the stiffnesses of braces and dampers were calculated by multiplying the values of α and β by the undamped frame stiffness. The undamped frame stiffness at each story was determined from static analysis. It is noted that the retrofit required strengthening of the outer columns in the damped bays (columns C-22, C-23, C-24, C-31, C-32, and C-33 in Fig. 5(c)) to carry the tension and compression forces on these columns (Fan [3], Lee [4]). The stiffness of the strengthened columns was considered when the undamped story stiffness was evaluated.

Elastic-static analysis procedure (ESAP)

With the brace and damper stiffnesses corresponding to the selected values of α and β, elastic-static analyses in Step (5) of the SDP were performed through the following elastic-static analysis procedure (ESAP) proposed by Fan [3] for VE dampers: (a) estimate the first-mode deflected shape under a pattern of equivalent lateral forces, (b) estimate the first-mode period using Rayleigh's method, (c) estimate the first-mode damping ratio, (d) determine the seismic coefficient from a design spectrum, (f) compute the equivalent lateral forces, (g) perform static analysis under the equivalent lateral forces to estimate the displacements, internal forces, and deformations of the damped system, and (h) correct the calculated response considering the simplifications of the analytical model.

The first-mode deflected shape and the first-mode period in Steps (a) and (b) of the ESAP can be estimated from static analysis using an inverse-triangular pattern of lateral forces, since the deflected shape of the damped system is intended to have a linear displaced shape under the design forces. In Step (c), the lateral force energy (LFE) method, proposed by Sause *et al.* [13], was used to estimate the first-mode damping ratio as follows:

$$\xi_{eq} = \frac{\eta_d}{2} \frac{\underline{P}_d^T \underline{u}_d}{\underline{P}^T \underline{u}} \tag{9}$$

where, η_d is the loss factor of the dampers, $\underline{P}_d$ is the vector of forces in the dampers, $\underline{u}_d$ is the vector of damper deformations, $\underline{P}$ is the vector of (inverse-triangular) applied static lateral forces, and $\underline{u}$ is the vector of corresponding first-mode lateral displacements at each floor. A value of η_d at 30°C was used in Eq. (9) as a lower bound because η_d generally becomes larger when the ambient temperature decreases.

The design spectrum of the International Building Code [14] was selected to represent the design basis earthquake (DBE). The damping ratio for a structure with dampers is higher than that of the design spectrum, developed assuming 5% damping, so that the design spectrum needs a modification using a damping reduction factor. The damping reduction factor (*DRF*) suggested in NEHRP-97 [15] was used to calculate the seismic coefficient from the design spectrum. In Step (f) of the ESAP, the equivalent lateral forces (*ELF*) are calculated as:

$$ELF = M\,\underline{u}\left(\Gamma \cdot DRF \cdot C_s \cdot g\right) \tag{10}$$

where, M is the mass matrix, $\underline{u}$ was defined for Eq. (9), Γ is the participation factor, and C_s is the seismic coefficient, and g is the acceleration due to gravity. C_s is the minimum of $S_{D1}/(T \cdot R/I)$ and $S_{DS1}/(R/I)$, where T is the estimated first-mode period in Step (a) of the ESAP, R is the response modification factor, and I is the occupancy modification factor. S_{DS} and S_{D1} are coefficients that define the design basis earthquake. The prototype RC frame building was assumed to be in Los Angeles, and values of S_{DS} and S_{D1} equal to

1.0g and 0.6g were used. The response modification factor R was assumed equal to 1 because the desired structural performance of the damped system is to remain elastic under the DBE.

Instead of using Eq. (10), the equivalent lateral force can be calculated using the vertical distribution factor defined by the International Building Code [14]:

$$ELF = C_{vx} \cdot V \text{ and } C_{vx} = \frac{w_x h_x^k}{\sum_{i=1}^{n} w_i h_i^k} \tag{11}$$

where, C_{vx} is the vertical distribution factor at level x, h_i and h_x is the height from the base to level i and x, w_i and w_x is the portion of the total gravity load located at level i and x, k is a distribution exponent related to the building period, and V is the base shear. A well-damped system will have a linear displaced shape. Therefore, for damped systems, k is assumed equal to 1, regardless of the period of the system. Then, Eq. (11) will produce results similar to results from Eq. (10), with an estimated first mode shape calculated using an inverse-triangular shape of lateral force.

It is important to note that the damper stiffness is assumed to be proportional to the undamped story stiffness, which is an elastic property. Therefore, the SDP and ESAP procedure ignores the damping stiffness of damper, leading to underestimation of internal forces. The amplification and modification factors proposed by Fan [3] were used in Step (h) of the ESAP to amplify the damper forces considering the damping stiffness. The axial forces in the columns in the damped bays also need to be amplified because these columns transmit the damper forces to the foundation. Other member forces such as moment and shear in the beams and columns do not need to be amplified because these forces are directly related to the lateral displacement of the frame under the equivalent lateral force.

Upon completion of the ESAP, the structural responses for each β are compared to the design limits, and the minimum β, which satisfies the design limits, is determined in Step (7) of the SDP. Since elastomer and VE damper stiffer as the temperature decreases, this minimum β corresponds to the high-end temperature at the design temperature range (e.g., 30°C for the current study). Step (8) of the SDP investigates the structural response at the low-end temperature (e.g., 10°C). When the structural response at the low-end temperature satisfies the design limits, the design is completed with a determination of the damper area and thickness in the Step (9).

Simplified design results

Fig. 6(a) shows the variation of the first-mode periods of the damped RC frame building, determined in Step (b) of the ESAP, as β varies with a constant value of α equal to 30. Fig. 6(b) shows the equivalent viscous damping ratios (ξ_{eq}) of the three damped systems. The ISD-110 damped system has the greatest ξ_{eq} because the loss factor of ISD-110 material is the largest. The equivalent lateral forces (ELFs), evaluated in Step (f) of the ESAP, are shown in Fig. 6(c) for the UHDNR damped system.

The story drift responses obtained from the ESAP are shown in Fig. 6(d) for the UHDNR damped system. As shown, the story drifts greatly decrease as β increases. For the UHDNR damped system, β values of 3.0 are required to keep the second story drift (the largest) less than the drift limit of 0.4% in accordance with the second retrofit design limit. For the ISD-110 and KRATON-107 damped systems, β values to satisfy the drift limit are 1.0 and 3.0 respectively.

The column responses from the ESAP are shown in Fig. 7 and Fig. 8. Fig. 7 shows the column axial force-moment demand (P_d-M_d) responses of all columns in the interior damped frame for the UHDNR damped system. The factored capacities are also shown. As seen, the moment responses, essentially induced by the

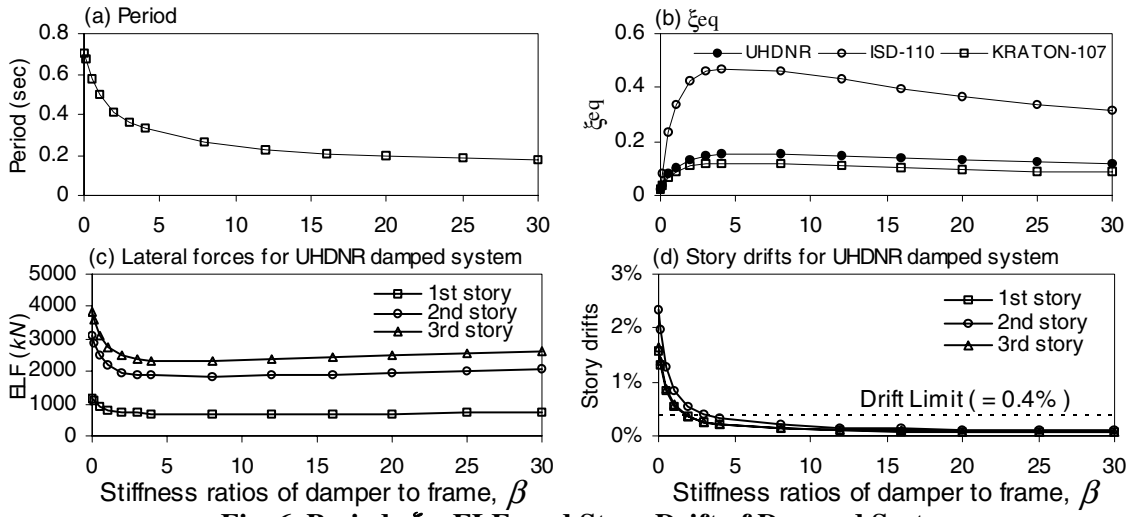

Fig. 6 Period, ξ_{eq}, ELF, and Story Drift of Damped Systems

story drifts, greatly decrease as β increases. Among all columns, the critical column is column C-36, which is located at the right end of the third story in the interior damped frame (See Fig. 5(c)). A β value of 8.5 is necessary for the response of this column to fall within the factored capacity curve. The β value of 8.5 will enable column C-36 to satisfy the first design limit, but this value is considered too large and impractical. The moment response for column C-36 was determined at the top of the column where the axial force and shear are not substantial. Instead of the moment at top end of the column, the moment at the bottom end was used for the retrofit design to reduce β. Then, the next critical column is column C-35 located just below column C-36. For this column, the required β is 3.8 to satisfy the first retrofit criterion. This β value may be more feasible. The required β values were determined from column C-35, and equal to 1.8 and 4.2 for the ISD-110 and KRATON-107 damped systems.

Fig. 8 shows the column axial force-shear demand (P_d-V_d) responses of columns C-34, C-35, and C-36 for the UHDNR damped system. The factored capacities are also shown. It was observed that the P_d-V_d responses calculated for the required β values, determined from the P_d-M_d response (i.e., β = 3.8, 1.7, and 4.5 for UHDNR, ISD-110, and KRATON-107), fall within the capacity curves for all columns.

From the simplified design, it is concluded that the retrofit design is governed by the P_d-M_d responses of the columns rather than the P_d-V_d responses or the story drifts. The required β values are 3.8, 1.7, and 4.8 for the UHDNR, ISD-110, and KRATON-107 damped systems, respectively, to satisfy the retrofit design limits. The required values of β, given above, are assumed to be at 30°C in the design temperature range of 10°C to 30°C, when the damping materials are the most flexible. The period, equivalent viscous damping ratio, story drift, and column C-22 axial force, which is subjected to the largest axial force demand, at 30°C are summarized in Table 2.

Table 2. Structural properties and story drifts determined from SDP

System	Temp (°C)	β	T_1 (sec.)	ξ_{eq}	Story Drift (%)			Column C-22 Axial Force (*kN*)	
					1st	2nd	3rd	Compression	Tension
UHDNR	30	3.8	0.34	0.15	0.22	0.34	0.23	2337.0	1007.0
	10	4.9	0.31	0.16	0.19	0.30	0.20	2363.7	1032.8
ISD-110	30	1.7	0.44	0.40	0.22	0.34	0.23	1904.6	592.9
	10	49.0	0.16	0.10	0.06	0.10	0.07	2821.4	1539.0
KRATON -107	30	4.8	0.32	0.12	0.22	0.33	0.23	2477.5	1165.8
	10	5.6	0.30	0.12	0.19	0.28	0.20	2564.3	1007.0

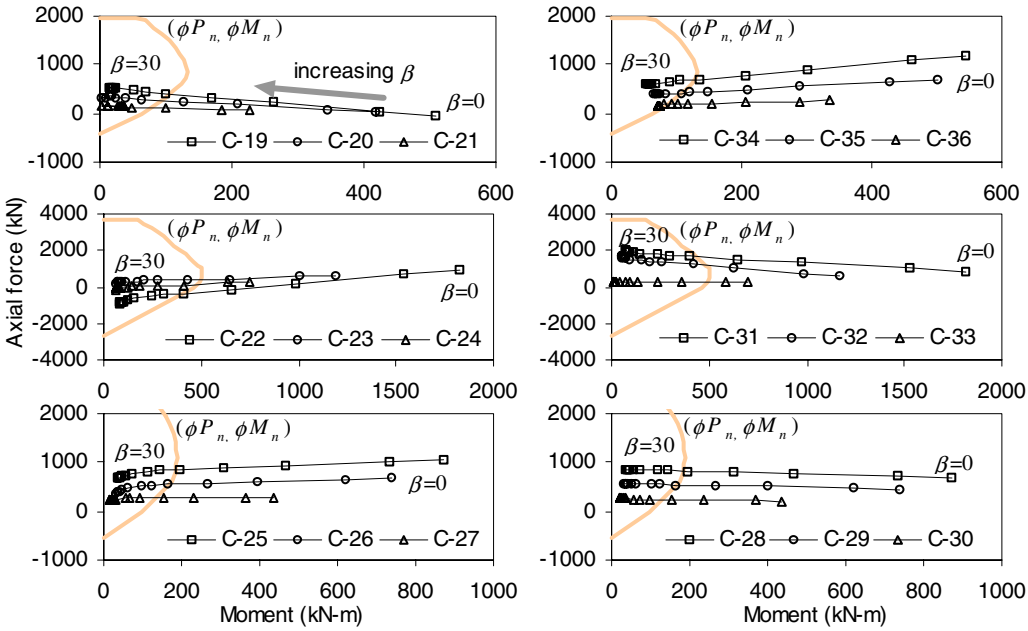

Fig. 7 Column P_d-M_d responses of UHDNR damped system

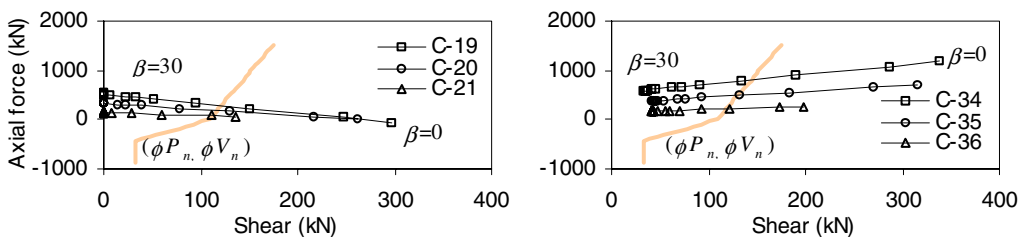

Fig. 8 Column P_d-V_d responses of UHDNR damped system

Estimated Seismic performance at 10 ℃

According to Step (8) of the SDP, the seismic performance at 10°C should be verified considering temperature-sensitive mechanical properties of the damping materials. The value of β_{10} (β at 10°C) can be obtained from the value of β_{30} (β at 30°C) by solving the following equation (Fan [3]):

$$\beta_{10} = \frac{G'\left(temp_{10}, \omega_{10}(\beta_{10})\right)}{G'\left(temp_{30}, \omega_{30}(\beta_{30})\right)} \beta_{30} \tag{12}$$

where, $G'(temp, \omega)$ is the elastic shear modulus of the damping material as a function of temperature and frequency, $temp_{10}$ equals 10°C, $\omega_{10}(\beta_{10})$ is the frequency of the damped system at 10°C as a function of β_{10}, $temp_{30}$ equals 30°C, and $\omega_{30}(\beta_{30})$ is the frequency of the damped system at 30°C as a function of β_{30}.

The values of β_{10} determined from Eq. (12) are 4.9, 49.0, and 5.6 for the UHDNR, ISD-110, and KRATON-107 damped systems. The significant increase in β value is observed for the ISD-110 damped system because the ISD-110 is highly sensitive to ambient temperature and frequency.

With these β_{10} values at 10°C, the period, damping ratio, story drift, and column member behaviors can be obtained from Fig. 6 through Fig. 8 without performing the elastic-static analyses again. Table 2 summarizes the period, ξ_{eq}, story drift, and column C-22 axial force at 10°C. Compared to the response at 30°C, the story drifts at 10°C are always smaller due to the larger damper stiffness at 10°C. However, the column C-22 axial force in ISD-110 damped system, increases significantly. Except this large axial force, the seismic responses of the three damped systems at 10°C satisfy the design limits.

Nonlinear dynamic time history analyses

A total of 54 nonlinear dynamic time history analyses (NDTHAs) were performed to verify the seismic performance anticipated from the SDP. As shown in Table 3, nine ground motions were selected and scaled to an intensity similar to the DBE, represented by the 5% damped IBC 2000 design spectrum [14]. Table 3 compares the pseudo-acceleration, S_{pa}, for each ground motion at the first-mode period and damping ratio of each damped system at 30°C, with that for the DBE, $C_{s,DBE}$.

Table 3. Ground motions

Identifier	EQ Name, Station	Component	Scale Factor	$S_{pa}/C_{s,DBE}$		
				UHDNR	ISD-110	Kraton-107
ART	Artificial		1.00	1.09	0.92	0.99
BOL	Duzce, Turkey (1999) Bolu	BOL000	0.74	1.61	1.07	1.50
ELC	EL Centro (1940) Imperial Valley	NS	1.39	0.99	1.25	0.90
LA11	Loma Prieta (1989) Gilroy #3	fn-45	1.07	0.87	0.82	0.97
LA14	Northridge (1994) Newhall	fn-45	0.62	1.16	1.04	1.18
LA21	Kobe (1995)	fn-45	0.46	1.15	1.51	0.96
LPG	Loma Prieta (1989) 47381 Gilroy #3	G03090	1.10	0.93	0.71	1.06
NRC	Northridge (1994) Canoga Park	CNP196	1.26	1.57	1.74	1.41
NRS	Northridge (1994) Saticoy St.	STC180	0.80	1.19	1.09	1.06

Seismic performance at 30℃ observed from NDTHAs

The maximum story drifts for the UHDNR damped system at 30°C under the nine ground motions are shown in Fig. 9(a). Except the second story drift under the BOL and NRC ground motions, the story drifts satisfy the drift limit (0.4%). The mean and mean plus standard deviation of the maximum story drifts obtained from the nine ground motions are shown in Figs. 9(b), (c), and (d) for each damped system. These mean maximum story drifts are well below the design drift limit and agree well with the story drifts determined from the SDP.

The P_d-M_d responses for columns C-34, C-35, and C-36, that controlled the retrofit design, are shown in Fig. 10(a) for the UHDNR damped system under the BOL ground motion and in Fig. 10(c) for the ISD-110 damped system under the NRC ground motion. As shown in Table 3, these ground motions are the most demanding ground motions for both systems with S_{pa}-to-$C_{s,DBE}$ ratios equal to 1.61 and 1.74 respectively. In the figures, two axial force-moment capacities, P_n-M_n and P_n-M_{ys} are shown to compare the response with the capacities. M_n is the nominal moment capacity, and M_{ys} is the moment when the

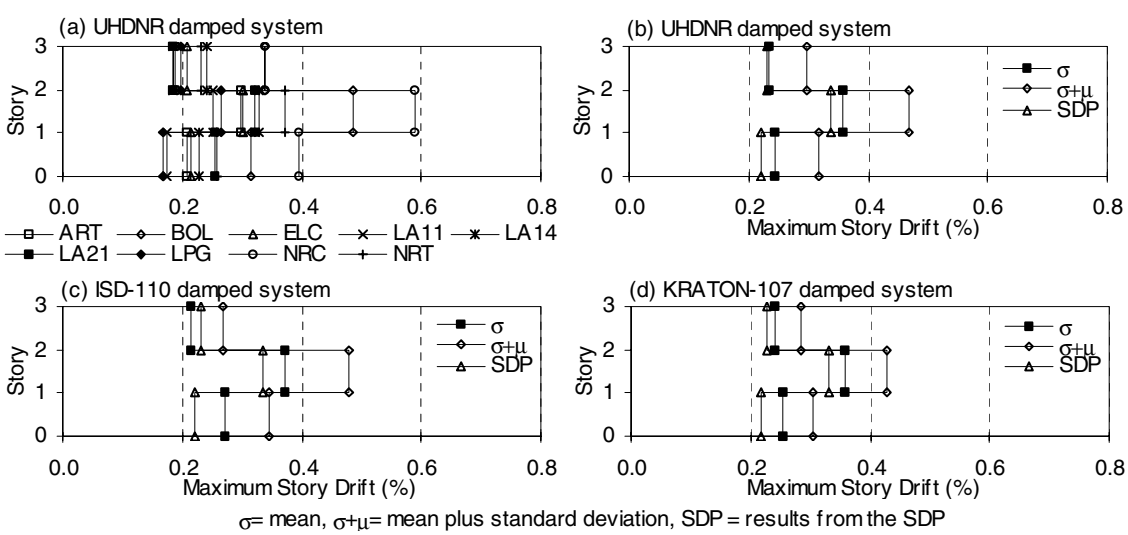

Fig. 9 Maximum story drift from NDTHAs

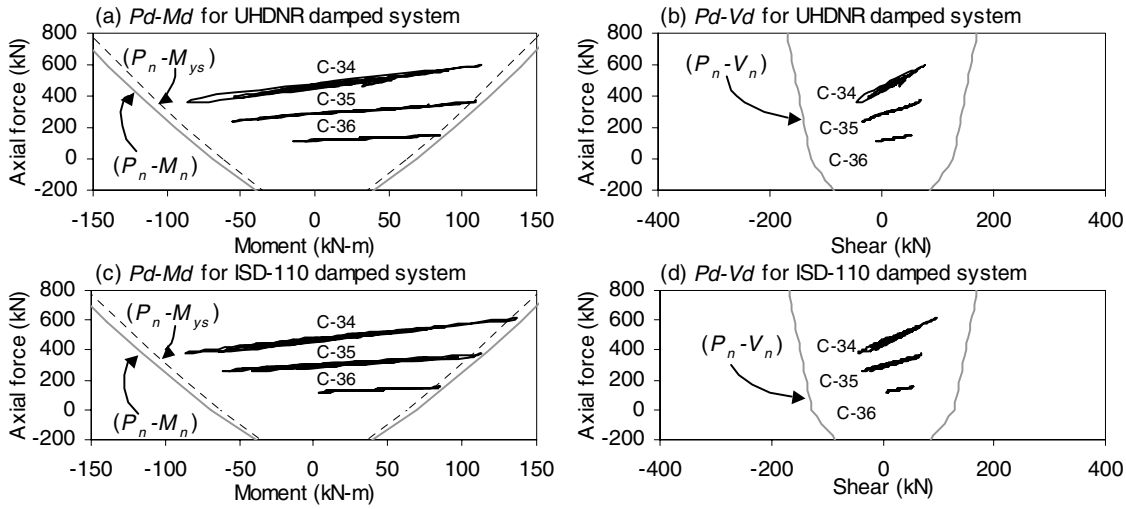

Fig. 10 Column P_d-M_d and P_d-V_d responses from NDTHAs

longitudinal steel bars in tension yield. Columns with P_d-M_d responses outside of the P_n-M_n capacities are considered to have failed in axial compression-flexure. As shown, all P_d-M_d responses are within the P_n-M_n capacity. However, P_d-M_d is outside of the P_n-M_{ys} curve including minor yielding for some columns. Despite this minor yielding, a similar investigation for all columns concluded that axial compression-flexural failure did not occur in the three damped systems under the nine ground motions.

The P_d-V_d responses for columns C-34, C-35, and C-36 are shown in Fig. 10(b) for the UHDNR damped system under the BOL ground motion and in Fig. 10(d) for the ISD-110 damped system under the NRC ground motion. The P_n-V_n capacity is shown to compare the response with the capacity. A brittle shear failure is assumed if the P_d-V_d response exceeds the P_n-V_n capacity. As expected from the SDP, the P_d-V_d is well within the P_n-V_n capacity. Brittle shear failure did not occur under the nine ground motions.

Seismic performance at 10℃ observed from NDTHAs

Nonlinear time history analyses were performed at 10°C to investigate the temperature dependence of the damping materials on the seismic response. As observed from the SDP at 10°C, the damping materials have larger stiffness and damping at lower temperatures, leading to smaller story drift, moment, and shear force demands. However, the axial force responses of some columns, especially the outer columns in the damped bays such as columns C-22 and C-32, are significantly increased.

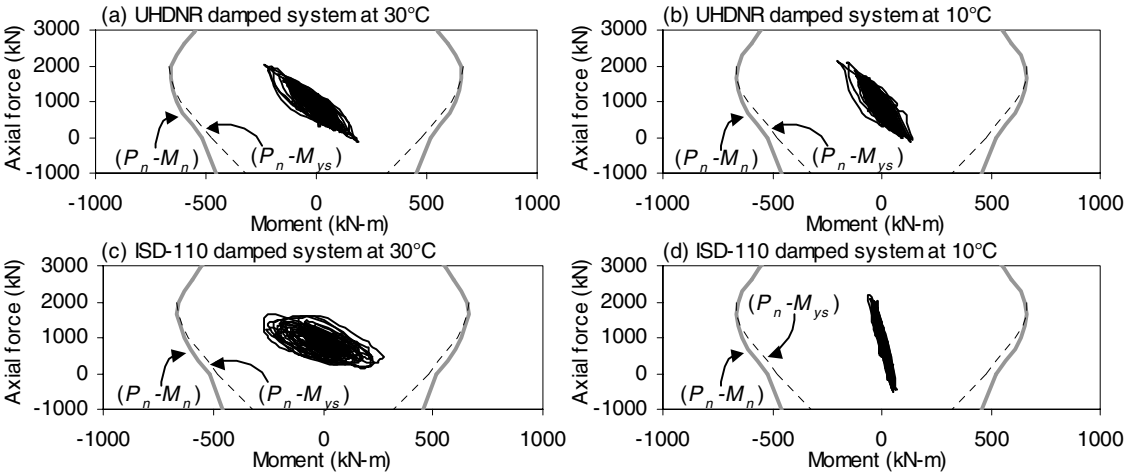

Fig. 11 Column C-22 axial force-moment responses at 30°C and 10°C

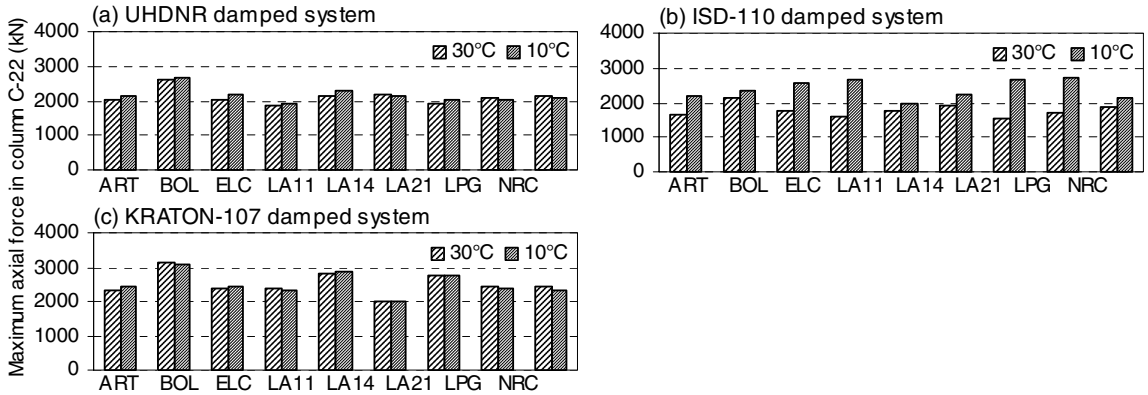

Fig. 12 Comparison of maximum axial force in column C-22

Fig. 11 compares the P_d-M_d responses of column C-22 for the UHDNR and ISD-110 damped systems under the ART ground motion at 30°C and 10°C. The P_d-M_d responses of column C-22 in the UHDNR damped system are similar at the two temperatures because the damping materials are nearly insensitive to temperature. As shown in Fig. 11(c) and (d), the P_d-M_d response of column C-22 of the ISD-110 damped system is quite different at the two temperatures. The P_d-M_d response at 10°C has much larger force and less energy dissipation than at 30°C.

The maximum axial forces in column C-22 under the nine ground motions are shown in Fig. 12. Since the retrofit does not strengthen the foundation, which was originally designed for gravity load only, excessive axial force in the columns is a potential problem. As shown, the maximum axial forces in column C-22 of the ISD-110 damped system vary significantly when temperature changes from 30°C to 10°C, while those of the UHDNR and KRATON-110 damped systems do not change significantly. A 36% increase in the maximum axial force of column C-22 is observed for the ISD-110 damped system from the nine ground motions. In the other hand, only a 2% change in maximum axial force is observed from the UHDNR and KRATON-107 damped systems.

CONCLUSIONS

A rate-dependent hysteretic model is presented to simulate the nonlinear hysteretic behavior of elastomer dampers. The model is composed of the generalized polynomial asymptote and power function model (PAPFM) parallel with a dashpot so that the strain dependent and loading rate dependent behavior can be simulated together. The rate-dependent hysteretic model compares well with the experiments.

To illustrate the improved seismic performance of non-ductile RC frame buildings that can be obtained by retrofit with elastomer dampers, a retrofit study was conducted. The simplified design procedure (SDP) determines the most effective damper properties based on global and local member performances. The UHDNR, ISD-110, and KRATON-107 retrofit systems were designed to remain essentially elastic under the DBE level ground motions.

The nonlinear dynamic time history analyses (NDTHAs) verify that the expected story drifts and member forces from the SDP agree well with those observed from the NDTHAs. Minor yielding occurred in some columns under ground motions more demanding than the DBE, but the columns have a reserve strength and deformation capacity, neither axial compression-flexural nor brittle shear failure is observed for the three damped systems.

At 30°C, the maximum responses, including the story drift, axial force, moment, and shear force demands

of the UHDNR, ISD-110, and KRATON-107 retrofit systems are similar to those expected from the SDP. Considering the axial force demand at 10°C, the temperature-insensitive UHDNR damper outperforms the ISD-110 damper, which outperforms the KRATON-107 damper. The ISD-110 material, with the largest loss factor outperforms the other two materials at 30°C, however it becomes too stiff at 10°C, resulting in excessive axial force demands on the columns. The KRATON-107 material may not be appropriate for a structural damping material because its loss factor of 0.29 is too low.

ACKNOWLEDGEMENTS

This research was conducted at the Center for Advanced Technology for Large Structural Systems (ATLSS) at Lehigh University. The authors acknowledge the support of the Malaysian Rubber Board and the PA Department of Community and Economic Development through a grant to the Pennsylvania Infrastructure Technology Alliance. The findings, opinions, and conclusions expressed in the paper are the authors and do not necessarily reflect the opinions of those acknowledged here.

REFERENCES

1. Chang, K. C., Soong, T. T., Lai, M. L., Oh, S.-T. "Seismic Behavior of Steel Frame with Added Viscoelastic Dampers," *Journal of Structural Engineering*, ASCE, Vol. 121, 1995: pp. 1418-1426.
2. Kasai, K., Fu, Yaomin "Passive Control Systems for Seismic Damage Mitigation," *Journal of Structural Engineering*, ASCE, 1998: Vol. 124, pp. 501-512.
3. Fan, C.P. "Seismic Analysis, Behavior, and Retrofit of Non-Ductile Reinforced Concrete Frame Buildings with Viscoelastic Dampers," Ph.D. Dissertation, Department of Civil and Environmental Engineering, Lehigh University, 1998.
4. Lee, K.-S. "Seismic Behavior of Structures with Dampers Made from Ultra High Damping Natural Rubber," Ph.D. Dissertation, Department of Civil and Environmental Engineering, Lehigh University, 2003.
5. Sause, R., Lee, K.-S., Ricles, J., Ab-Malek, K., Lu, L.-W. "Non-linear Hysteresis Models for Ultra-high Damping NR Structural Dampers," *Journal of Rubber Research*, Vol. 4, 2001.
6. Marquardt, D.M. "An algorithm for least-squares estimation of nonlinear parameters," *J. Soc. Indust. Appl. Math.*, 11, 1963: 431-441.
7. Wu, S. "Seismic Performance and Retrofit of Non-Ductile Reinforced Concrete Frame Structures," Ph.D. Dissertation, Department of Civil and Environmental Engineering, Lehigh University, 1995.
8. Farahany, M.M. "Computer Analysis of Reinforced Concrete Cross Sections," M.S. Thesis, The University of Texas at Austin, 1977.
9. Blume, J.A., Newmark, N.M., Corning, L.H. "Design of Multistory Reinforced Concrete Buildings for Earthquake Motions," *Portland Cement Association*, Chicago, 1961.
10. Kent, D.C., Park, R. "Flexural Members with Confined Concrete," *Journal of Structural Engineering*, ASCE, 1971: Vol. 97(7), pp. 1969-1990.
11. Habibullah, A., Wilson, E. "SAP 2000: Integrated Finite Element Analysis and Design of Structures," Computers and Structures Inc., Berkeley, CA, 1997.
12. Maison, B.F. "PC-ANSR: Microcomputer Program for Nonlinear Structural Analysis," NISEE, University of California, Berkeley, CA, 1992.
13. Sause, R., Hemingway, G.J., Kasai, K. "Simplified Seismic Response Analysis of Viscoelastic-Damped Frame Structures," *Proceedings, 5th U.S. National Conference on Earthquake Engineering*, EERI, 1994: Vol. I, pp. 839-848.
14. ICC "*International Building Code*" International Code Council (ICC), Falls Church, VA, 2000.
15. NEHRP Guidelines for the Seismic Rehabilitation of Buildings, *Report No. FEMA-273*, Federal Emergency Management Agency, Building Seismic Safety Council, Washington, D.C., 1997.